A Direct Conversion Transceiver for Portable Microfluidic NMR Flowmeters

Aydin, Eren; Jouyaeian, Amirhossein; Tang, Zhong; Makinwa, Kofi

DOI
10.1109/ESSERC62670.2024.10719403

Publication date
2024

Document Version
Final published version

Published in
ESSERC 2024 - Proceedings

A Direct Conversion Transceiver for Portable Microfluidic NMR Flowmeters

Eren Aydin, Amirhossein Jouyaeian, Zhong Tang and Kofi Makinwa
Electronic Instrumentation Laboratory, Delft University of Technology, Delft, The Netherlands
Email:e.aydin@tudelft.nl

2024 IEEE European Solid-State Electronics Research Conference (ESSERC) | 979-8-3503-8813-8/24/$31.00 ©2024 IEEE | DOI: 10.1109/ESSERC62670.2024.10719403

***Abstract*— This paper presents a direct conversion transceiver intended for use in a microfluidic NMR flowmeter. It consists of an H-bridge power amplifier, which drives a hand-wound milimeter-sized coil with RF signals, and a direct conversion receiver, which amplifies the NMR signals picked up by the coil, and then digitizes them with an asynchronous 8-bit SAR ADC sampling at 70MHz. Fabricated in a 65nm CMOS technology, the receiver achieves a noise spectral density of 1 nV/sqrt(Hz) at 21 MHz, while dissipating only 36 mW. A microfluidic flowmeter based on the transceiver and a handheld 0.5 T permanent magnet can measure flow rates up to 96 ml/h in a 0.8mm inner-diameter channel with ±1.3% full-scale error. To the authors' best knowledge, this is the first reported portable NMR flowmeter.**

Keywords*— NMR, ASIC, CMOS, flowmeter, direct-conversion, ADC, transceiver

I. Introduction

Nuclear magnetic resonance (NMR), referring to the resonant interaction of nuclei with an RF magnetic field (B_1) in the presence of a static magnetic field (B_0), is widely used in applications ranging from healthcare to chemistry [1]. However, its adoption in portable applications is limited by bulk and cost considerations. Over the last two decades, however, NMR systems have become steadily smaller, mainly due to advances in the development of permanent magnets [2] and NMR transceivers [3] [4] [5] [6] [7]. Benchtop NMR systems are now commercially available, while handheld NMR systems for certain applications, such as point-of-care detection [8], have been demonstrated. NMR flowmeters [9] [10], however, have not yet been miniaturized despite their advantages over conventional flowmeters.

NMR flowmeters operate by exploiting the movement of magnetized fluid through the excitation/detection coil of an NMR system, which systematically alters the resulting NMR signals. Flow rate can then be accurately determined by analyzing these signals without the need for physical contact, making NMR flowmeters ideal for a wide range of applications. For example, they can be used to sense the flow of corrosive or scalding fluids without disturbing the flow profile or sample integrity. Furthermore, in contrast to other types of flow sensors, they can also be used to perform fluid composition analysis. Conventional NMR flowmeters are quite bulky and so have only been used in large-scale applications [10]. Recently, it has been shown that by using permanent magnets and low-noise electronics, significantly smaller systems can be realized [11]. However, the portability of such systems is still limited by the size of the magnet and its PCB-based electronics.

This paper presents a highly miniaturized NMR flowmeter based on an NMR transceiver implemented in a standard 65 nm CMOS process. The transmitter consists of an H-bridge power amplifier, which drives the coil to excite the fluid sample at RF frequencies. With a 3.3V supply, it can deliver a maximum current of 200 mA to the coil. The receiver features a signal chain that consists of an ultra-low-noise amplifier, followed by an 8-bit SAR ADC. The receiver dissipates 36 mW of power from a 1.2 V supply and exhibits a spectral noise density of 1 nV/sqrt(Hz) at 21 MHz. Together with a compact 0.5 T permanent magnet, the transceiver is the key component of an NMR flowmeter, whose key components only occupy some 200 cm^3, and weighs less than 1 kg.

This paper is organized as follows: In Section II, flow measurement using the NMR principle will be introduced, while Section III discusses the state-of-the-art of integrated NMR transceivers and compares them to the proposed architecture. In section IV, experimental results are presented. Finally, the paper will be concluded by highlighting potential applications and future research directions.

II. Flow Measurement Using NMR

In NMR flowmeters, as in magnetic resonance imaging (MRI) systems, the requirements on magnetic field homogeneity, and hence the need for complicated magnet designs and additional gradient and shimming coils, can be somewhat relaxed by the use of Carr-Purcell (CP) pulse sequences. Flow speed can then be derived from the decay in the peak amplitudes of the resulting NMR echos [10].

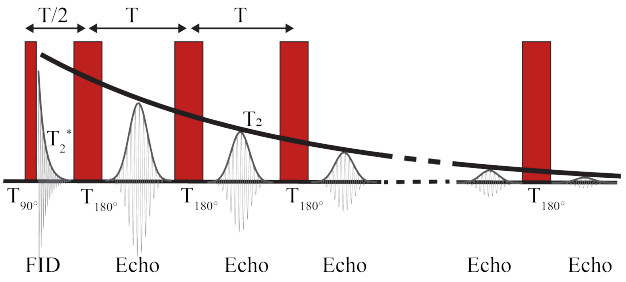

Fig. 1. Illustration of CP pulse sequence; the red rectangles represent the RF excitation moments. When the field homogeneity decreases, the bandwidth of the NMR signal increases, which causes faster decay, so-called T_2^*. Applying the CP pulse sequence, which consists of a T90° pulse followed by a train of T180° pulses, allows the T_2 decay to be accurately estimated from the peaks of the echo signals.

As shown in Fig. 1, applying CP pulses to a fluid results in a typical so-called T_2 pattern, whose envelope exhibits an exponential decay. In the presence of flow, this decay is accelerated by the movement of the magnetized fluid volume away from the RF detection coil. This results in an additional decay component *f(t)*, which is dependent on the flow rate. Although T_2 decay is fluid dependent, *f(t)* can be made fluid independent by normalizing the measured decay under no-

flow conditions, called T_2 normalization (Fig. 2). As shown in Eq. 1, the slope of *f(t)* is then a linear function of flow speed, in which a and b are fitting coefficients.

$$f(t) = -at + b \tag{1}$$

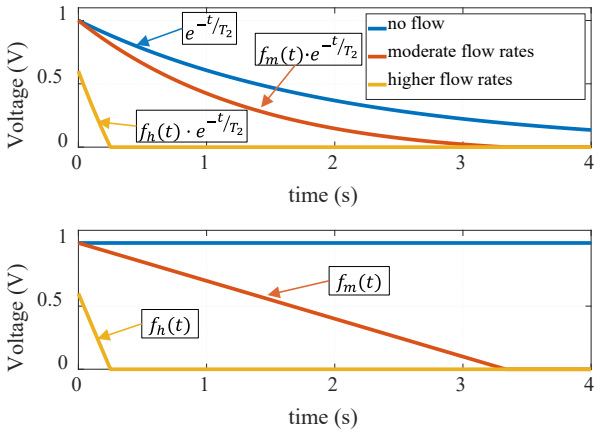

Fig. 2. Illustration of the effect of flow on NMR signals (top) and T_2 normalization concept (bottom). The NMR signal's amplitude decreases when the flow rate increases due to their shorter exposure to the B_0 field, resulting in fewer protons.

The flow rate is then proportional to the normalized slope of the obtained *f(t)*, which is given by:

$$flow\ rate \propto normalized\ slope = -\frac{a}{b} \tag{2}$$

III. Proposed Architecture

State-of-the-art low-field NMR transceivers are typically based on the architecture shown in Fig. 3. Depending on their level of integration, they comprise H-bridge power amplifiers (PAs), TX/RX switches, low-noise amplifiers (LNA, analog I/Q demodulators, IF amplifiers, and ADCs. However, demodulating NMR signals to an IF frequency requires frequency offsetting [3], the use of additional local oscillators (LO) [6], or frequency switching between TX and RX cycles [7]. These methods all result in trade-offs, which in [3] compromise excitation efficiency, in [6] require an extra LO, and in [7] require the use of a frequency-shift-keying scheme.

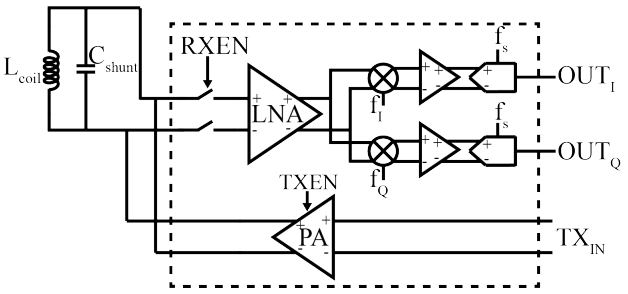

Fig. 3. A typical NMR transceiver schematic based on analog IQ demodulation.

Since NMR signals are quite small (~10 µV), NMR receivers typically have gains ranging from 60 to 100 dB, depending on coil size and sample volume. Most of this gain is located after their IF demodulators, since it is more efficient to create gain at low frequencies. As a result, such receivers may be potentially saturated by offset, either due to amplifier mismatch or to self-mixing effects in their IF demodulators. To address this, DC servo loops (DSLs) are often employed, which increases system complexity.

In low-IF NMR receivers based on I/Q demodulators , the phase and amplitude mismatch of the I and Q channels will lead to signal reconstruction errors. To address this, multi-temperature calibration is often required, which again increases cost. Another approach, called CYCLOPS [12], mitigates mismatch by averaging the results of two consecutive NMR measurements made with swapped I and Q channels. However, it also doubles the required measurement time.

Driven by the increasing efficiency of high-speed ADCs, the current trend in RF systems is to eliminate IF stages and directly digitize RF signals. This approach circumvents the typical issues of I/Q demodulation such as slow settling and channel mismatch. Furthermore, the use of digital signal processing offers increased flexibility.

However, direct digitization methods have yet to be adopted in portable NMR transceivers. To fill this gap, we propose the NMR transceiver shown in Fig. 4. As before, the coil is driven by a H-bridge PA, while the receiver employs a simplified signal chain that consists of a cascade of amplifiers followed by an 8-bit asynchronous SAR ADC. The external C_{shunt} is tuned to match the coil's resonance frequency with the Larmor frequency to amplify the thermal noise and the NMR signal together and relax the noise specification of the receiver [3].

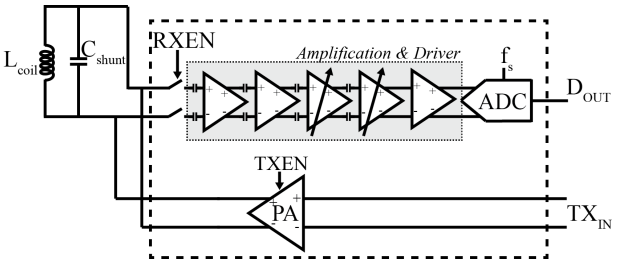

Fig. 4. The schematic of the proposed system.

The receiver employs a chain of four amplifiers capable of providing a total gain ranging from 60 to 90 dB. Each amplifier consists of open-loop gm-stages with resistive loads, which are AC coupled to each other. The resulting HP filters dictate the receiver's settling time constant. To prevent signal attenuation, the coupling capacitors are considerably larger than the input capacitance of each stage. Finally, the amplified NMR signal is digitized by an 8-bit asynchronous SAR ADC. To maintain good linearity, the output swing of the amplifier chain is limited to ~600 mV_{pp}. To match this range with a 1.2V reference, the ADC's sampling network employs an attenuating capacitor, as in [13]. Its capacitive DAC (CDAC) consists of 0.75 fF unit capacitances made from single-layer fringe capacitors, which is sufficient to achieve 8-bit matching [14].

The digital output of the transceiver was then acquired by an external logic analyzer with a sampling frequency of f_s=71.43 MHz, and then demodulated with the digital IQ demodulation scheme shown in Fig. 5.

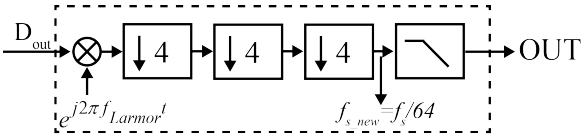

Fig. 5. The digital IQ demodulation and low-pass filtering block diagram. The digital output was demodulated to DC (zero-IF demodulation) before any filtering operation. The demodulated signal was decimated by a factor of 64 and filtered using an 8th-order Butterworth filter.

IV. Experimental Results

A micrograph of the designed chip, implemented in TSMC 65 nm standard CMOS, is illustrated in Fig. 6. The chip occupies an area of 2.2 mm². Subsequently, the fabricated chip is wire-bonded to a plastic 44-pin 7 mm x 7 mm QFN package.

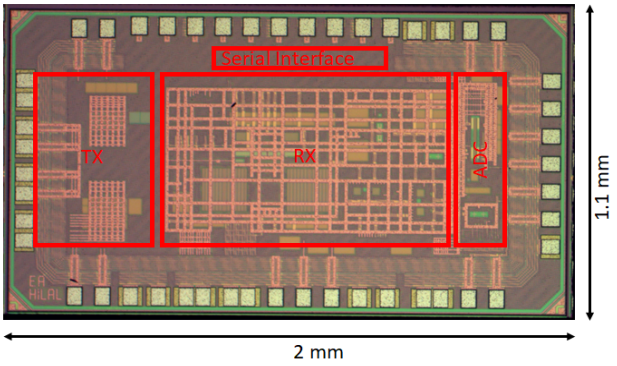

Fig. 6. The micrograph of the fabricated chip

A. Characterization of the Transceiver

The input referred noise of the receiver result is shown in Fig. 7. The IRN at 21 MHz is 1nV/sqrt(Hz), which is sufficiently lower than the coil's noise at its resonance frequency, 21 MHz, to ensure minimal effect on the NMR signals. The receiver dissipates 36 mW, including the pad drivers of the ADC. Specifically, the analog front-end consumes 33.6 mW, with the first stage accounting for the majority at 21.6 mW. The ADC and its pad drivers dissipate 2.4 mW.

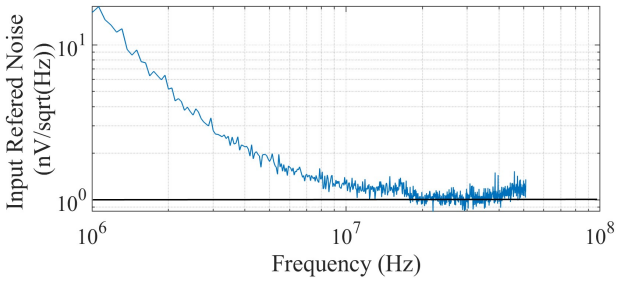

Fig. 7. The IRN of the receiver

The transmitter was tested by connecting a 5 Ω resistor and applying a square wave at 21 MHz. Subsequently, the voltage across the 5 Ω resistor was measured, as illustrated in Fig. 8, which indicates that the transmitter has a driving capability exceeding 200 mA_p.

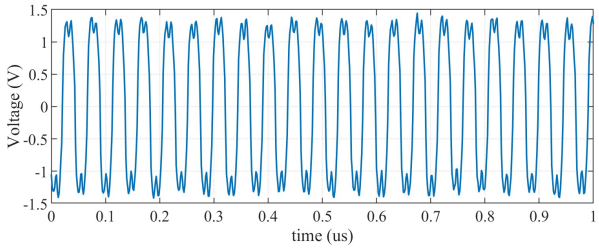

Fig. 8. Transmitter output voltage when loaded with a 5 Ω resistor

B. Flow Measurements

A handheld magnet shown in Fig. 9 (left) [2] was utilized for the flow measurements. This magnet measures only 8 cm long, with a 5 mm gap for sample insertion, and weighs just 400 grams. Specifically designed for flow measurement, this magnet features a homogeneous region at the end where the coil is inserted, allowing more time for sample magnetization. The magnet has a B_0 of 0.495 T and a nominal Larmor frequency for ^1H (f_{Larmor}) of 21.1 MHz. A 6 mm-long coil wound around a PTFA tube with an inner diameter of 0.8 mm, using enamel-coated copper wire with a diameter of 0.25 mm. The sample volume inside the coil under static conditions is 3 µL. Although the NMR signals from this sample look noisy due to the lower sample volume and inferior homogeneity, the T_2 decay can still be accurately measured.

The setup for the flow measurement is depicted in Fig. 9 (right). The coil was placed inside the magnet and soldered close to the ASIC. The digital output of the ASIC was read out using a logic analyzer, and the ASIC itself was controlled by a DAQ (Data Acquisition) board. The flow rate is regulated by a mass-flow controller through a falcon pressurized with 4 bars pressure, with its flow rate data serving as the reference for our flow measurements.

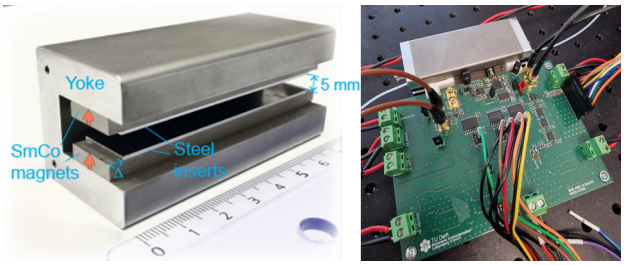

Fig. 9. The photograph of the handheld magnet specifically designed for flow measurement (left), The photograph of the test setup (right)

NMR experiments were conducted for 2 seconds, ranging from static conditions to a flow rate of 96 ml/h. The measured NMR signals are depicted in Fig. 10. Following the T_2 normalization process, the NMR signals appear as illustrated in Fig. 11. The normalized slopes of these signals were calculated by fitting a line to each other, employing Eq. 2. Subsequently, the obtained normalized slope values were mapped to the flow rate using a first-order polynomial. Consequently, the proposed flowmeter exhibits a ±1.3% full-scale error (Fig. 12) comparable with commercially available flowmeters.

C. Benchmarking

The proposed NMR transceiver introduces a novel receiver architecture for portable NMR devices. By

employing open-loop amplifiers and a high-speed ADC, it becomes feasible to achieve efficiency comparable to low-IF IQ demodulator-based NMR transceivers while attaining significantly faster settling times. Table 1 compares the performance of the proposed chip with the recently published NMR ASICs, and it can be seen that the proposed ASIC achieves state-of-the-art performance.

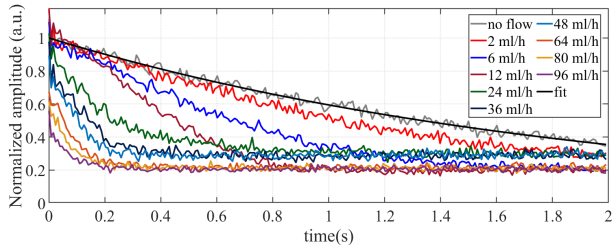

Fig. 10. NMR signals obtained with different flow rates from 0 to 96 ml/h.

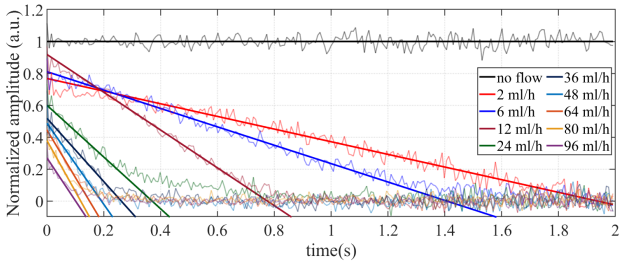

Fig. 11. The T_2 normalized signals (faint and noisy plots) and fitted lines on the T_2 normalized signals (clear plots.)

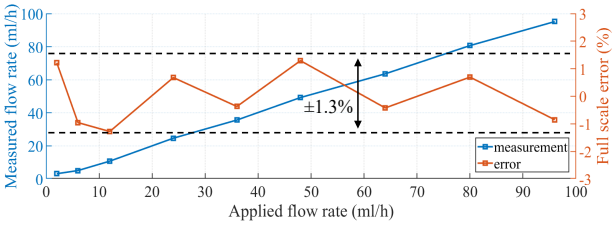

Fig. 12. Measured flow rate (left y-axis, straight lines) and full-scale error

TABLE I.
PERFORMANCE COMPARISON WITH THE STATE OF THE ART

Specifications	[4]	[5]	[6]	[7]	This work
Process	180 nm	180nm HVSOI	180 nm	180 nm	65 nm
Radio Tech.	Low-IF IQ	Low-IF IQ	Low-IF IQ	Low-IF IQ	Direct Conv.
Larmor Freq. (MHz)	21	22	21.07	10-60	21.1
IRN	0.67	0.8	0.95	0.75	1
Settling time	-	-	10 µs	-	<1 µs
Power Diss. (mW)	47	-	36	43	36
TX Driving Cap. (mA)	860	1280	-	290	200
RX Gain Range (dB)	30-110	-	65-125	30-100	60-90
Chip area	5.6	4.1	1.8	5	2.2

V. CONCLUSION

This paper describes a portable NMR flowmeter, which is based on a compact NMR transceiver realized in a standard 65 nm CMOS process. Its portability and non-contact measurement capability, make it well-suited for use in chemistry, healthcare, and microfluidics applications. The proposed NMR transceiver employs a direct conversion receiver, which enhances system performance and usability by reducing the time needed to eliminate IQ channel mismatch. Future research may focus on the integration of digital transmitters into NMR transceivers for true software-defined portable NMR, simplifying usage with microcontrollers or FPGAs, and further enhancing and expanding capabilities in NMR technology.

ACKNOWLEDGMENT

This work is a part of the research program FLOW+ under project number 15025, which is co-funded by the Netherlands Organization for Scientific Research (NWO), Bronkhorst High-Tech, and Krohne.

REFERENCES

[1] "NMR and MRI Applications in Chemistry and Medicine - National Historic Chemical Landmark - American Chemical Society." Accessed: Apr. 09, 2024. [Online]. Available: https://www.acs.org/education/whatischemistry/landmarks/mri.html

[2] D. Polishchuk and H. Gardeniers, "A compact permanent magnet for microflow NMR relaxometry," *Journal of Magnetic Resonance*, vol. 347, p. 107364, Feb. 2023.

[3] N. Sun, Y. Liu, H. Lee, R. Weissleder, and D. Ham, "CMOS RF Biosensor Utilizing Nuclear Magnetic Resonance," *IEEE J. Solid-State Circuits*, vol. 44, no. 5, pp. 1629–1643, May 2009.

[4] A. Zhang et al., "A Wideband CMOS NMR Spectrometer for Multinuclear Molecular Fingerprinting," in 2023 *Symp. VLSI Circuits*, pp. 1–2, Jun. 2023,.

[5] S. Fan, Q. Zhou, K. M. Lei, R. P. Martins, and P.-I. Mak, "17.2 A Miniature Multi-Nuclei NMR/MRI Platform with a High-Voltage SOI ASIC Achieving a 134.4dB Image SNR with a 173×250×103µm 3 Resolution," *Digest of ISSCC*, pp. 316–318, Feb. 2024.

[6] S. Hong and N. Sun, "Portable CMOS NMR System With 50-kHz IF, 10-µs Dead Time, and Frequency Tracking," *IEEE Transactions on Circuits and Systems I: Regular Papers*, vol. 68, no. 11, pp. 4576–4588, Nov. 2021.

[7] D. Krüger et al., "A Portable CMOS-Based Spin Resonance System for High-Resolution Spectroscopy and Imaging," *IEEE J. Solid-State Circuits*, vol. 58, no. 7, pp. 1838–1849, Jul. 2023.

[8] J. Anders and K. Lips, "MR to go," *Journal of Magnetic Resonance*, vol. 306, pp. 118–123, Sep. 2019.

[9] M. Meribout, "Optimal Design for a Portable NMR- and MRI-Based Multiphase Flow Meter," *IEEE Transactions on Industrial Electronics*, vol. 66, no. 8, pp. 6354–6361, Aug. 2019.

[10] T. M. Osán et al., "Fast measurements of average flow velocity by Low-Field ^{1}H NMR," *Journal of Magnetic Resonance*, vol. 209, no. 2, pp. 116–122, Apr. 2011.

[11] E. Aydin and K. A. A. Makinwa, "A Low-Field Portable Nuclear Magnetic Resonance (NMR) Microfluidic Flowmeter," *21st International Conference on Solid-State Sensors, Actuators and Microsystems(Transducers)*, pp. 1020–1023, 2021.

[12] D. Reichert and G. Hempel, "Receiver imperfections and CYCLOPS: An alternative description," *Concepts Magn Reson*, vol. 14, no. 2, pp. 130–139, Jan. 2002.

[13] P. J. A. Harpe et al., "A 26 µW 8 bit 10 MS/s Asynchronous SAR ADC for Low Energy Radios," *IEEE J. Solid-State Circuits*, vol. 46, no. 7, pp. 1585–1595, Jul. 2011.

[14] V. Tripathi and B. Murmann, "Mismatch characterization of small metal fringe capacitors," *Proceedings of the IEEE 2013 Custom Integrated Circuits Conference*, IEEE, pp. 1–4, Sep. 2013.